(2)

SECURITY CLASSIFICATION OF THIS PAGE (When Data Entered)

REPORT DOCUMENTATION PAGE

READ INSTRUCTIONS BEFORE COMPLETING FORM

1. REPORT NUMBER: 18660.2-PH	2. GOVT ACCESSION NO.: AD-A129931
3. RECIPIENT'S CATALOG NUMBER: N/A	
4. TITLE (and Subtitle): Excimer Laser Photolysis Studies of Translational-to-Vibrational Energy Transfer in Collisions of H and D Atoms with CO	5. TYPE OF REPORT & PERIOD COVERED: Reprint
	6. PERFORMING ORG. REPORT NUMBER: N/A
7. AUTHOR(s): Charles A. Wight, Stephen R. Leone	8. CONTRACT OR GRANT NUMBER(s): DAAG29 82 K 0030
9. PERFORMING ORGANIZATION NAME AND ADDRESS: University of Colorado, Boulder, CO 80309	10. PROGRAM ELEMENT, PROJECT, TASK AREA & WORK UNIT NUMBERS: N/A
11. CONTROLLING OFFICE NAME AND ADDRESS: U. S. Army Research Office, P. O. Box 12211, Research Triangle Park, NC 27709	12. REPORT DATE: 15 Apr 83
	13. NUMBER OF PAGES: 12
14. MONITORING AGENCY NAME & ADDRESS(if different from Controlling Office)	15. SECURITY CLASS. (of this report): Unclassified
	15a. DECLASSIFICATION/DOWNGRADING SCHEDULE

16. DISTRIBUTION STATEMENT (of this Report)

Submitted for announcement only.

DTIC ELECTE JUL 1 1983 S D B

17. DISTRIBUTION STATEMENT (of the abstract entered in Block 20, if different from Report)

18. SUPPLEMENTARY NOTES

19. KEY WORDS (Continue on reverse side if necessary and identify by block number)

20. ABSTRACT (Continue on reverse side if necessary and identify by block number)

83 06 30 102

DD FORM 1 JAN 73 1473 EDITION OF 1 NOV 65 IS OBSOLETE

Unclassified

SECURITY CLASSIFICATION OF THIS PAGE (When Data Entered)

Excimer laser photolysis studies of translational-to-vibrational energy transfer in collisions of H and D atoms with CO

Charles A. Wight and Stephen R. Leone[a)]

Joint Institute for Laboratory Astrophysics, National Bureau of Standards and University of Colorado, and Department of Chemistry, University of Colorado, Boulder, Colorado 80309
(Received 3 December 1982; accepted 7 January 1983)

Translational-to-vibrational excitation of carbon monoxide is observed as a result of collisions of high energy H and D atoms with CO. The fast atoms are produced by excimer laser photolysis of H_2S, D_2S, HCl, HBr, or HI at 193 or 248 nm. Detection of time and wavelength-resolved infrared fluorescence is used to quantify the CO vibrational state excitation. The CO ($v = 1 - 6$) state distribution from H (H_2S, 193 nm, $E_{cm} = 2.3$ eV) + CO collisons is 0.74 ± 0.15, 0.15 ± 0.01, 0.08 ± 0.01, 0.01 ± 0.01, 0.02 ± 0.01, and 0.01 ± 0.01. The corresponding state distribution from D (D_2S, 193 nm, $E_{cm} = 2.2$ eV) + CO is 0.79 ± 0.19, 0.13 ± 0.01, 0.05 ± 0.02, 0.02 ± 0.02, 0.01 ± 0.01, and 0.01 ± 0.01. Rotational excitation is at least as significant as vibrational excitation, based on estimates of the total energy transfer. Measurements of the relative vibrational excitation efficiency as a function of initial H atom energy show that the fraction of translational energy converted to CO vibration increases by more than 300% as the initial H atom energy is increased from 1.0 to 3.2 eV. Good qualitative agreement is found between the experimental results and classical trajectory calculations carried out for collinear collisions of H and D atoms with CO using a simple repulsive interaction potential.

I. INTRODUCTION

Energy transfer between translational and internal degrees of freedom plays an important role in the characterization of excitation and relaxation mechanisms in energetic environments such as chemical reactors or plasmas. Interest in this area has been high because developments in new lasers, laser-selective chemistry, and laser isotope separation are often critically dependent on the control of energy transfer pathways. Many studies have explored vibration-to-translation (V–T) energy transfer by monitoring vibrational relaxation rates in various gases as a function of temperature.[1] On the other hand, most information concerning translation-to-vibration (T–V) energy transfer has come from molecular or ion beam scattering and energy loss spectroscopy. Excellent reviews of both V–T[2–4] and T–V[3,5,6] energy transfer studies have been published.

Recently, a new technique for investigating T–V excitation was simultaneously developed in our laboratory[7] and at Brookhaven National Laboratory by Quick, Weston, and Flynn.[8] Fast hydrogen atoms with energies of 1–3 eV are produced by excimer laser photolysis of a diatomic or triatomic hydride. Collisions of these fast atoms with other molecules in a flow tube can excite molecular vibrations directly, or in some cases can induce chemical reactions leading to vibrationally excited products. The vibrational excitation is monitored by observing infrared emission from $\Delta v = -1$ transitions. By recording the time and wavelength-resolved emission following the photolysis laser pulse, earlier studies obtained the population distribution in excited vibrational states of HCl following collisions with fast H atoms.[7] The fraction of excited HCl molecules that is produced by nonreactive T–V excitation and reactive H atom exchange has been determined in a subsequent study by investigation of H + DCl and D + HCl collisions.[9]

Here, we have undertaken an investigation of inelastic collisions between H atoms and CO. These collisions are different from the previous H + HCl cases because the CO bond strength is sufficient to prevent chemical reactions under these conditions. One of the most interesting aspects of this study is that although no chemical reactions with CO can occur, the H + CO collision takes place on the potential energy surface corresponding to the bound free radical HCO, where chemical forces can play a potentially significant role in determining the collision and energy transfer dynamics. The influence of this attractive surface on V–T energy transfer was recently examined in a shock tube study of CO vibrational relaxation in collisions with atomic hydrogen.[10] The results were interpreted in terms of intramolecular vibrational relaxation during the lifetime of the HCO intermediate complex. Chemical forces have also been implicated in inelastic scattering[11] of protons with CO. A theoretical study[12] has shown that the strong attraction between H^+ and CO can lead to sharp features in the energy-dependent scattering cross sections. The resonances are attributed to compound state formation in a relatively long-lived HCO^+ complex. At the high translational energies in our T–V experiment (1.0–3.2 eV), it is unlikely that the HCO collision complex lives for more than one or two CO vibrational periods, but the influence of chemical forces on the T–V energy transfer dynamics is a definite possibility.

Several results of investigations of CO collisions with fast hydrogen atoms are described. Population

[a)]Staff Member, Quantum Physics Division, National Bureau of Standards.

 0021-9606/83/084875-12$02.10

distributions for excited CO vibrational states are determined for H_2S and D_2S photolysis at 193 nm where the initial energy of the H (D) atom is 2.3 (2.2) eV in the center-of-mass frame of the T–V collision. A semiquantitative estimate of the total CO vibrational excitation is made at other initial H atom energies by using various other H atom precursors and photolysis laser wavelengths. The results are compared with classical trajectory calculations computed for collinear collisions of H and D atoms with CO using a simple repulsive potential. Finally, an estimate is made for the total efficiency of energy transfer for the translational-to-vibrational and rotational excitation of the CO molecules.

II. EXPERIMENTAL SECTION

A. Apparatus and techniques

The basic experimental technique involves the photolytic production of translational excited H atoms and wavelength-resolved infrared detection of molecular emission to determine the extent of vibrational excitation in the CO target molecules. A dilute mixture of the H atom precursor (H_2S, HCl, HBr, or HI) in carbon monoxide is pumped through a 30 mm diam glass flow tube past the laser photolysis region by a liquid-nitrogen-trapped mechanical pump (Fig. 1). The excimer laser beam enters and exits the photolysis region through fused silica windows mounted on the sides of the tube with 25 mm O-ring joints. Infrared fluorescence is viewed by an infrared detector through a MgF_2 window mounted directly above the path of the laser beam.

The initial H atom translational energy is determined by conservation of energy and momentum for photolysis of the diatomic precursors (Table I). Photodissociation of HBr and HI produces significant amounts of spin-orbit excited halogen atoms at the wavelengths used,[7,13] resulting in bimodal distributions of initial H atom energies. Hawkins and Houston have shown by laser-induced fluorescence of SH that photolysis of H_2S at 193 nm results in a nearly monoenergetic distribution of H atom energies since very little excess energy appears as vibrational or rotational excitation in the HS fragment.[14] The H atoms rapidly lose translational energy in collisions with CO so that the observations are the result of the first main collision and one or two successive collisions at drastically lower energies.

TABLE I. Initial H and D atom translational energies from excimer laser photolysis.

Precursor	λ^{laser}(nm)	$E_{c.m.}$(eV)[a]
HI	193	3.19 (>90%); 2.29 (<10%)[b]
HBr	193	2.51 (85%); 2.14 (15%)[c]
H_2S	193	2.30
D_2S	193	2.16
HCl	193	1.84
HI	248	1.82 (50%); 0.91 (50%)[b]
H_2S	248	0.95

[a]H atom translational energy in the center-of-mass frame of an H + CO collision; laboratory frame energies are approximately 4% greater.

[b]The two energies result from the two I atom channels, $I^*(^2P_{1/2})$ and $I(^2P_{3/2})$. The quantum yield for production of $I^*(^2P_{1/2})$ atoms is from Ref. 13.

[c]The two energies result from the two Br atom channels, $Br^*(^2P_{1/2})$ and $Br(^2P_{3/2})$. The quantum yield for $Br^*(^2P_{1/2})$ atoms is from Ref. 7.

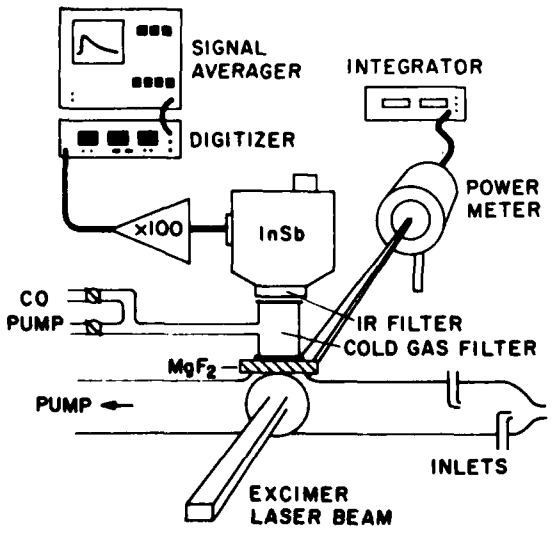

FIG. 1. Schematic drawing of the experimental apparatus showing the photolysis cell, cold gas filter cell, infrared detector, and signal processing equipment.

For most experiments with the H_2S precursor, a premixed sample of 5% H_2S in CO is used in order to keep the partial pressure of H_2S in the flow tube as constant as possible over long experimental run times. Prior to sample preparation, H_2S is degassed and purified by vacuum distillation at −113 °C. Carbon monoxide, reagent or technical grade, is slowly passed through a 1.5 m length of copper tubing immersed in liquid nitrogen to remove condensible impurities such as CO_2. There is no detectable difference in the results when the two grades of CO are purified in this manner. Hydrogen atom precursors other than H_2S are purified by degassing and vacuum distillation. They are mixed with purified CO directly in the flow tube at 5% concentration. The relative concentrations of precursor and CO are monitored by gas flow meters in the inlet lines. The meters are calibrated with each gas before and after each experiment. In some experiments, the relative concentration of added helium buffer gas is also monitored in this manner. The total pressure of the mixture in the flow tube is measured with a capacitance manometer mounted a few centimeters downstream of the photolysis region. Typical total pressure is 7 Pa (1 Pa = 7.5×10^{-3} Torr).

The photolysis source is a rare gas halide excimer laser operated at 193 or 248 mm. A small portion of the beam is sampled by a photodiode, which is used to trigger the signal acquisition electronics. The remainder of the unfocused laser beam is tightly masked before it passes through the flow tube to keep stray in-

frared light produced in the laser discharge from reaching the detector. A volume absorbing power meter behind the flow tube monitors the average laser power transmitted through the cell. The voltage output of the power meter is integrated so that the observed infrared fluorescence signals may be averaged for many laser pulses and later corrected for small variations in the total laser energy for each run. The laser is typically operated at ten pulses per second with pulse energies in the cell of 15 and 60 mJ at 193 and 248 nm, respectively. The beam area is approximately 1.5 cm^2 as it passes through the cell.

Two different infrared detectors are used to monitor the infrared fluorescence from vibrationally excited CO molecules. For wavelength-resolved measurements, a 0.3×1.0 cm copper-doped germanium (Ge:Cu) detector cooled with liquid helium is used. A 77 K circular variable interference filter (CVF) with 2 mm slits transmits a narrow (50–60 cm^{-1} FWHM) range of wavelengths in the region of interest and blocks room temperature blackbody light. The bandpass of the filter may be continuously varied by rotating the filter wheel past the slits. In this way, a low resolution infrared emission spectrum of CO is obtained from 1900–2300 cm^{-1}. The 77 K background radiation from the filter assembly is greatly attenuated by a 4 K MgF_2 window mounted between the filter and detector element to block wavelengths longer than 10 μm.

In order to deconvolute an emission spectrum, the response characteristics of the filter/detector combination must be carefully measured. First the transmission spectrum of the CVF is determined at several different positions. The Ge:Cu detector is illuminated with infrared radiation from a hot Chromel wire which is dispersed into a 10 cm^{-1} band with a 0.5 m monochromator. The output of the detector is monitored as the monochromator is scanned across the filter transmission region. To determine the sensitivity per photon of the filter/detector combination, the flux of a reference blackbody emitter is measured as a function of the CVF setting. The output of the detector is compared with the calculated blackbody transmission through the CVF to construct a curve of relative sensitivity vs CVF setting.

The second detector used in this study is a liquid-nitrogen cooled 1.27 cm^2 InSb detector equipped with a fixed frequency room temperature bandpass filter which transmits the entire CO emission spectrum. This detector has higher overall sensitivity because of its large area and is used to make both the measurements of relative emission intensity vs initial H atom energy and the intensity ratios of $CO(v=1)$ to total $CO(v)$ emission. Both detectors are used in conjunction with a 1 cm pathlength cold gas filter cell equipped with sapphire windows and mounted between the photolysis region and the infrared detector. This cell is evacuated to transmit all of the emission or is filled with 15–65 kPa of CO at room temperature to absorb all of the $v=1 \rightarrow v=0$ emission. The cell has sapphire windows and may also be filled with CO_2 to test for the possible presence of emission from this impurity at 4.3 μm. A second similar cell with a 2.5 cm pathlength was used in some experiments.

The output signal from either of the infrared detectors is amplified and recorded by a fast transient digitizer (2048 channels, 10 ns/channel minimum). A 250 kHz or 1 MHz low pass electronic filter is inserted between the amplifier and digitizer to reduce the high frequency detector noise when the fastest response of the detector is not required. The digitized signal is immediately transferred to a digital signal averager where signals from 500–5000 laser pulses are summed to improve the signal-to-noise ratio. A hard copy of the final averaged signal is obtained on an X–Y chart recorder and the digitized signal is transferred to a microcomputer for storage and further numerical analysis.

B. Methodology for determining vibrational populations

If the pressure of carbon monoxide in the flow tube is above about 7 Pa, self-absorption of the $v=1 \rightarrow 0$ emission causes an apparent reduction in the emission intensity and a distortion of the low resolution band shape. The distortion is due to preferential absorption of the emission associated with the lower rotational levels since these are more populated. In addition to keeping the CO pressure low, it is desirable to keep the partial pressure of the H_2S precursor molecules at or below 5% in order to avoid collisions of H atoms with H_2S during the T–V excitation. Unfortunately, the signal-to-noise ratio at pressures of CO low enough to prevent self-absorption is too poor to spectrally resolve the emission band shape with the Ge:Cu detector and circular variable interference filter. The excited vibrational state populations are therefore determined in two steps.

In the first part, a cold gas filter with 15–65 kPa of CO is mounted between the flow cell and the detector to remove all of the emission from $v=1 \rightarrow 0$. Self-absorption of emission from higher levels is negligible, so the pressure of the CO in the experimental cell may be increased to about 70 Pa. Above this pressure the vibration-to-vibration relaxation rates of the $CO(v)$ come too close to the response time of the detector and signal acquisition electronics. A low resolution spectrum of emission for levels $v \geq 2$ is then obtained by recording the time-resolved emission at many different CVF settings. With the spectroscopic constants[15] and transition moments[16,17] of CO and the measured detector characteristics, the emission spectrum is deconvoluted to determine the relative populations for the vibrational states $v \geq 2$. The deconvolution procedure is outlined in the following section.

In the second part of the population measurement, the relative population of the $v=1$ level is determined with the InSb detector by measuring the emission intensity in the presence and absence of the CO cold gas filter. The signal-to-noise ratio in this experiment is large enough that the pressure of CO in the experimental cell may be reduced to a point where self-absorption is negligible. The intensity observed with the cold gas cell filled is divided into its various $v \geq 2$ components using the previously determined relative populations.

TABLE II. Rotationless vibrational transition dipole moments and Einstein coefficients for $\Delta v = -1$ transitions in CO.

v	R^v_{v-1}(D)	$A_{v,v-1}(s^{-1})^c$
1	0.1040[a]	33.4
2	0.147[a]	64.3
3	0.179[a]	91.8
4	0.206[a]	116.9
5	0.238[b]	150.1
6	0.259[b]	170.9

[a]Reference 16 (Young and Eachus).
[b]Reference 17 (Weisbach and Chackerian).
[c]$A_{v,v-1} = 64\pi^4\nu^3 |R^v_{v-1}|^2/3h$.

The extra intensity observed when the cold gas cell is evacuated is then ascribed to emission from the $v=1$ level. The relative population in $v=1$ is given by

$$N_1 = \frac{B-C}{CA_1} \sum_{v\geq 2} N_v A_v \ , \tag{1}$$

where C and B are the intensities observed with and without the cold gas filter, respectively. The relative populations are N_v and the A_v are the respective Einstein coefficients for spontaneous emission. The Einstein coefficients used in this study are listed in Table II.

C. Spectral deconvolution procedure

Data for the spectral deconvolution are obtained by recording the time-resolved emission intensity at many different CVF wavelength settings. Several spectra may be constructed, each corresponding to a different delay time relative to the photolysis laser pulse. Each experimental spectrum is then fit in a least-squares procedure to a calculated spectrum corresponding to the sum of emission intensities from individual vibrational levels. The parameters to be obtained in this fit are the relative populations of the levels, N_v.

The calculated spectrum for each transition is obtained by first constructing a line spectrum consisting of the individual P and R branch transitions. The wavelengths are determined from the known Dunham coefficients for CO.[15] The intensities of the lines are given by

$$I_{vJ-v'J'} = \frac{64\pi^4\nu^3}{3h} |R^v_{v'}|^2 F_{vJ-v'J'}(J+J'+1) \frac{\exp(-E^{rot}_{vJ}/kT^{rot})}{Q^{rot}} \ , \tag{2}$$

where I has units of photons molecule^{-1} s^{-1}. The rotational dependence of the square of the vibrational transition dipole moment $|R^v_{v'}|^2$ is given by the Herman–Wallis factor $F_{vJ-v'J'}$ which is close to unity for $\Delta v = 1$ transitions in CO.[16] The form of Eq. (2) assumes a Boltzmann distribution of rotational levels characterized by a temperature T^{rot}. The line strength factor is given by $J+J'+1$, and E^{rot} and Q^{rot} are the rotational energy and partition function of the emitting level.

For each vibrational transition, the line spectrum is convolved with the measured CVF transmission function at every filter wavelength setting. The total calculated intensity at each setting is obtained by summing the intensities at each frequency ν_i for all the vibrational transitions weighted by their relative populations, viz,

$$I(\nu_i) = \sum_{v\geq 2} N_v I_v(\nu_i) \ . \tag{3}$$

The population deconvolution is accomplished by minimizing the sum of the squares of the deviations between calculated and experimental data points using the N_v as adjustable parameters. The minimization condition occurs when

$$\frac{d}{dN_k}\left\{\sum_i [I(\nu_i) - I^{expt}(\nu_i)]^2\right\} = 0 \tag{4}$$

for each N_k. The experimental emission intensity at each filter setting i is given by $I^{expt}(\nu_i)$ and the N_k are dummy variables for the vibrational populations. In this example, the vibrational indices v and k each take on values from 2 to the highest level produced in the T–V excitation. The $v=1$ level is not considered since the cold gas filter removes all of the intensity associated with that transition.

Substituting Eq. (3) into Eq. (4) and differentiating we obtain

$$\sum_v N_v\left[\sum_i I_v(\nu_i) I_k(\nu_i)\right] = \sum_i I^{expt}(\nu_i) I_k(\nu_i) \ . \tag{5}$$

This is a set of simultaneous equations in k with N_v as the unknowns and the term in brackets as the coefficients. In matrix notation this set of equations is expressed by

$$\mathbf{N}_v \cdot \mathbf{R}_{vk} = \mathbf{Z}_k \ , \tag{6}$$

where

$$R_{vk} = \sum_i I_v(\nu_i) I_k(\nu_i) \quad \text{and} \quad Z_k = \sum_i I^{expt}(\nu_i) I_k(\nu_i) \ .$$

Solving for N_v we have simply

$$\mathbf{N}_v = \mathbf{Z}_k \cdot (\mathbf{R}_{vk})^{-1} \ . \tag{7}$$

The computer program calculates $\mathbf{Z}$ and $\mathbf{R}$, inverts $\mathbf{R}$, and multiplies the result by $\mathbf{Z}$ to obtain the best fit populations.

III. RESULTS

A. Determination of vibrational populations

A time-resolved infrared signal obtained with the Ge:Cu detector at one filter wavelength setting is shown in Fig. 2. Because the H atoms have very high velocity, the collision rate is initially 10^8 s^{-1}. The rise time of the T–V signal is faster than the response time of the detector and electronics (1 μs) and appears to be complete during that time. Vibration-to-vibration energy transfer slowly reduces all of the higher vibrational states to $v=1$, which is invisible due to the presence of the cold gas filter. The fast decay at short times ($t < 5$ μs) following the laser pulse is due to relaxation of high rotational levels produced in the collisions of fast H atoms with CO. On the high and low frequency sides of the emission spectrum, production of the high J states results in this extra intensity at short times.

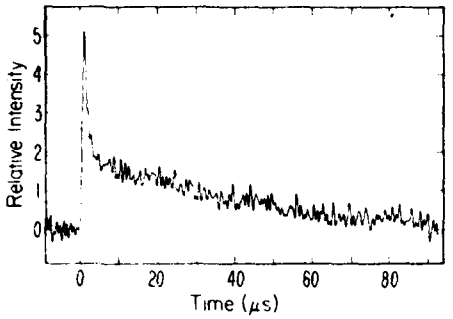

FIG. 2. Infrared emission signal from CO at 2205 cm^{-1} (filter transmission FWHM 60 cm^{-1}) following 193 nm photolysis of a 5% mixture of H_2S in CO. Total gas pressure in the photolysis cell is 66.7 Pa. The emission is viewed through a 2.5 cm long cold gas filter cell containing a 6.67 kPa of CO. Signals from 1000 pulses were averaged to obtain this trace. The initial rapid decay is due to high rotational states which are excited by the H atoms.

This extra intensity quickly decays away upon rotational relaxation. Toward the center of the emission spectrum the relative depletion of low J states causes a loss in intensity at short times and an apparent slowing of the rise time of the signal. At delay times longer than about 5 μs, the emission is consistent with a Boltzmann rotational state distribution throughout the spectrum.

Infrared signals at specific delay times are collected from runs at many different filter wavelength settings and normalized for small variations in laser energy. Small corrections are also made for variations in filter/detector sensitivity and window transmission functions. The data are then assembled to construct low resolution emission spectra such as the one in Fig. 3. Relative populations for the levels $v = 2$ are determined by the least-squares fitting procedure for several spectra corresponding to progressively longer delay times relative to the laser pulse. The deconvolution procedure, as described in the previous section, requires that the rotational state distribution be known. After the initial 5 μs, good fits are obtained using a room temperature Boltzmann distribution of rotational states. Extrapolation of the vibrational populations to $t = 0$ from the data after rotational relaxation is complete makes it unnecessary to assume the rotational populations at very short times. The extrapolation values reflect the vibrational populations after the T–V excitation is complete but before any appreciable vibrational relaxation has taken place.

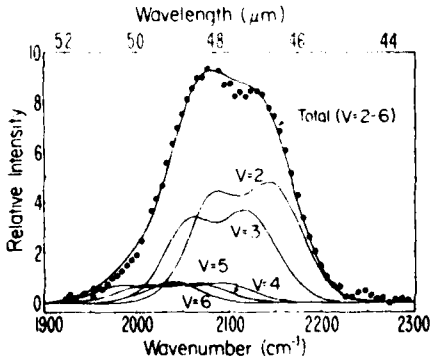

FIG. 3. Low resolution emission spectrum of CO. Experimental conditions are the same as in Fig. 2. Each point represents the observed emission intensity at 15 μs following the photolysis laser pulse. The solid line through the points is the best fit calculated emission spectrum from the vibrational population deconvolution procedure. Also shown are the contributions to the total spectrum from each of the vibrational levels $v = 2$–6.

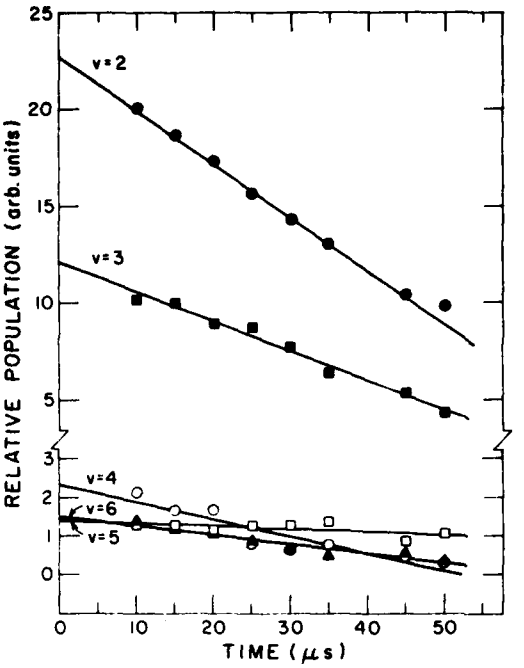

FIG. 4. Relative populations of the $v = 2$–6 levels vs time following the photolysis laser pulse. Experimental conditions are the same as in Figs. 2 and 3. Note the expanded vertical scale for the higher vibrational levels.

The relative populations in $v = 2$–6 are shown as a function of delay time for one run in Fig. 4. Vibrational levels from $v = 2$ to $v = 6$ are considered in the deconvolution program. Inclusion of higher levels has no significant effect on the results. Similar experiments are performed using D_2S to produce D atoms. The relative populations at zero delay time for the $v \geq 2$ levels are presented in Table III for the $H(H_2S)$ + CO and $D(D_2S)$ + CO experiments.

The relative contribution from $v = 1$ emission is determined by measuring the time-resolved emission using a broadband infrared filter to transmit the entire wavelength range of the CO($v = 1$–6) emission. Infrared signals measured with and without the cold gas filter are shown in Fig. 5. Both traces exhibit the expected fast initial rise time of the T–V excitation. The second trace (with the cold gas filter) shows the V–V relaxation of the $v \geq 2$ levels. The trace showing emission from all of the excited levels (without the cold gas filter) ex-

TABLE III. Summary of population deconvolution results for H + CO and D + CO T-V transfer.

Collision system	Detector	Relative populations[a]					
		$v=1$	$v=2$	$v=3$	$v=4$	$v=5$	$v=6$
H + CO	Ge:Cu	...	0.15 ± 0.01	0.07 ± 0.01	0.01 ± 0.01	0.03 ± 0.01	0.01 ± 0.01
H + CO	Ge:Cu	...	0.149 ± 0.03	0.078 ± 0.003	0.016 ± 0.003	0.010 ± 0.003	0.010 ± 0.003
H + CO	Ge:Cu	...	0.15 ± 0.01	0.08 ± 0.01	0.01 ± 0.01	0.01 ± 0.01	0.01 ± 0.01
H + CO	InSb	0.74 ± 0.15[b]					
D + CO	Ge:Cu	...	0.13 ± 0.01	0.06 ± 0.01	0.02 ± 0.01	0.00 ± 0.01	0.01 ± 0.01
D + CO	Ge:Cu	...	0.13 ± 0.01	0.04 ± 0.01	0.02 ± 0.01	0.01 ± 0.01	0.02 ± 0.01
D + CO	Ge:Cu	...	0.13 ± 0.01	0.04 ± 0.01	0.02 ± 0.01	0.02 ± 0.01	0.01 ± 0.01
D + CO	InSb	0.79 ± 0.19[c]					
H + CO	Final Populations	0.74 ± 0.15	0.15 ± 0.01	0.08 ± 0.01	0.01 ± 0.01	0.02 ± 0.01	0.01 ± 0.01
D + CO	Final Populations	0.79 ± 0.19	0.13 ± 0.01	0.05 ± 0.02	0.02 ± 0.02	0.01 ± 0.01	0.01 ± 0.01

[a] Quoted uncertainties are ± 1 standard deviation.
[b] $I(v=1)/I(v\geq 2) = 1.13 \pm 0.02$, six determinations.
[c] $I(v=1)/I(v>2) = 1.46 \pm 0.3$; ten determinations.

hibits a slight increase in intensity with time. This is because the higher vibrational levels cascade down to $v=1$ by V–V transfer. Each $v=n$ molecule produces n $v=1$ molecules which have a slightly higher total emission intensity than the original molecule. Depletion of the $v=1$ level by vibration-to-translation energy transfer occurs on a much longer time scale.

Evidence of extensive rotational excitation can again be seen as extra intensity at short times in Fig. 5(b). In the case of $\Delta v=1$ transitions in CO, the transition intensity varies only slightly with rotational quantum number. The extra intensity at short times is most likely due to transitions from high rotational levels of $v=1$ which are not blocked effectively by the cold gas filter. When helium buffer gas is added to the flow tube, the relaxation time associated with the high rotational levels becomes much shorter without significantly affecting the observed vibrational relaxation.

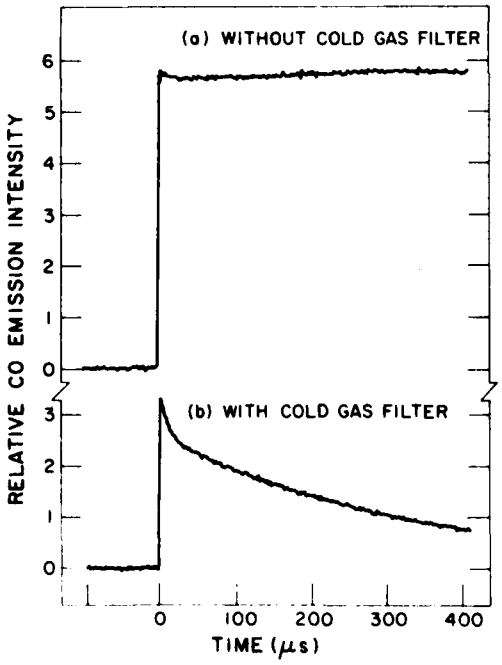

FIG. 5. Infrared emission signal from CO recorded with the InSb detector through a broad band infrared filter. Total pressure of the 5% H_2S/95% CO mixture in the photolysis cell is 8.0 Pa. Trace (a) was recorded by averaging signals from 1000 pulses (193 nm) with the cold gas filter cell evacuated. Trace (b) was recorded under identical conditions except with 57 kPa of CO in the cold gas filter cell to block emission from CO($v=1$). The extra intensity at $t<40$ μs is probably due to highly rotationally excited levels of $v=1$ which are not blocked by the cold gas filter.

The infrared intensities such as in Fig. 5 are extrapolated to $t=0$ disregarding the small intensity increase due to rotational excitation. The average ratio of the $v=1$ contribution to the $v\geq 2$ contribution was found to be 1.13 ± 0.2 for six determinations. Thus, slightly more than half of the total intensity is from $v=1$ molecules. The relative $v=1$ population is calculated to be 0.74 ± 0.15 from Eq. (1). Approximately half of the uncertainty in the $v=1$ population originates from uncertainties in the $v\geq 2$ populations. Experiments using D_2S as a D atom precursor yield results that are very similar to the H atom experiments. The populations of the $v\geq 2$ levels are determined in exactly the same way as the H atom experiments. The intensity ratio of $v=1/v\geq 2$ was found to be 1.46 ± 0.3 from ten cold gas filter measurements. Results for each of the spectral deconvolutions and intensity ratio measurements are summarized in Table III.

The vibrational population distributions are also presented in Fig. 6. It is immediately evident that the population distributions for H and D atom excitation are identical within the experimental uncertainty. In both cases, $v=1$ has the highest population and the excitation probability drops off sharply with the higher excited levels. Examination of the deconvoluted emission spectra, as in Fig. 3, shows that the intensity from the $v=5$ and 6 levels is significant although the uncertainty in the population is large. The apparent population inversion between $v=4$ and $v=5$ in the H + CO results is probably not significant. It is also important to note that there is no probe of the population remaining in $v=0$ in this experiment.

Although the population distributions for $v=1$–6 are

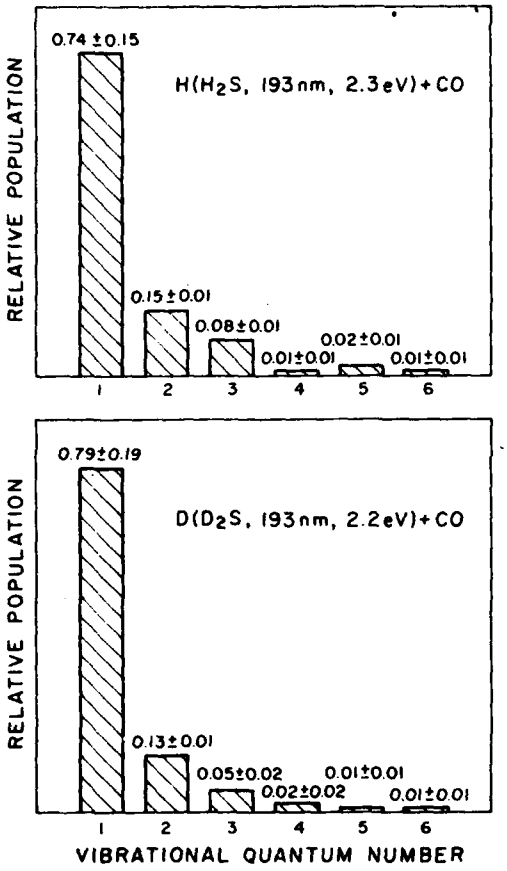

FIG. 6. Relative vibrational population distributions in CO(v= 1–6) following excitation by H and D atoms produced by 193 nm photolysis of H_2S and D_2S.

nearly the same for H or D atom excitation, the total emission intensity is found to be 2.8± 0.3 times greater with the H_2S precursor than with the D_2S precursor at an equal concentration. This difference cannot be attributed to a difference between the H and D atom yields. The average absorption cross section of four carefully prepared samples of D_2S was measured to be 7.6(± 0.1) $\times 10^{-18}$ cm^2, base e at 193 nm. Similarly, the cross section for H_2S at the same wavelength is 6.4(± 0.2) $\times 10^{-18}$ cm^2, which is in good agreement with the value of 6.6×10^{-18} cm^2 given by Watanabe and Jursa.[18] Since the same electronic transition is excited in H_2S and D_2S, it is unlikely that a difference in photodissociation quantum yield is responsible for the lower emission intensity in the D + CO experiments. Confirming experiments using the reaction $H + Br_2 \rightarrow HBr(v) + Br$ show that the relative yields of H and D atoms from H_2S and D_2S are the same as the relative absorption cross sections, within experimental uncertainty.

B. The nascent character of the populations

We first consider some of the sources of error in the overall population determination and estimate the uncertainty in the final results. Uncertainty in the infrared emission intensity stems from a number of sources including thermal background radiation, pressure fluctuations, fluctuations in the pulse energy of the photolysis laser, and imperfect reproducibility of the CVF setting. The signal-to-noise ratio for intensity vs time plots such as in Fig. 2 depends on the number of laser pulses that are averaged. For typical data used in the spectral deconvolutions (500 laser pulses per CVF setting) the uncertainty in the intensity at the peak of the emission spectrum near 2100 cm^{-1} is less than 10%. It is not easy to determine directly how noise in the spectra affects the uncertainty in the results of the population deconvolution. By evaluating the results at several different delay times, however, the uncertainty in the populations due to random errors is evident in Fig. 4. The extrapolations to $t = 0$ appear to be quite smooth, so the uncertainty in the intercept may be determined by the quality of the linear fits of population vs delay time (Fig. 4). In principle, the slope data in Fig. 4 contain information on the V–V deactivation rates of CO(v). The observed trend qualitatively agrees with the known V–V transfer rates.[19] A second major source of error stems from the intensity ratio measurements with and without the cold gas filter. The final intensity ratios given in Table III are averages of several determinations (six for H + CO; ten for D + CO), and the quoted uncertainties reflect the scatter in those measurements.

Several precautions are taken to eliminate systematic or nonrandom errors during data acquisition. Samples of H_2S (D_2S) and CO are premixed before the experiments so that the pressure ratio of the reagents remains constant during each run. The infrared detectors are allowed to cool for several hours before beginning an experiment to make sure that thermal equilibrium of the filters, and hence their final transmission spectral shift with temperature, is attained. For the wavelength-resolved measurements, data for one complete run are obtained by scanning the CVF through the emission region in big steps, but three or four times in the same direction. In this way, no two data points at adjacent wavelengths are taken consecutively. When cold gas filter measurements are made, the filter cell is evacuated and filled each time while in place so that the optical geometry remains undisturbed. For several runs, CO_2 is added to the cold gas filter to check against the possible presence of CO_2 impurity emission at 4.3 μm. This shows no discernible effect on the results, indicating that CO_2 emission is negligible.

It should be noted that the vibrational populations are dependent on the accuracy of the Einstein spontaneous emission coefficients used in the deconvolution and in Eq. (1). Further refinement of the Einstein coefficients in Table II will require modification of the populations listed in Table III.

In an experiment of this type, ideally one would like to determine the probabilities of exciting individual vibrational states for a single collision at a well-defined energy. Some aspects of this experiment cause the observed state distributions to be slightly different from those of the ideal experiment; these are not errors, *per se*, but a limitation of the technique which should be

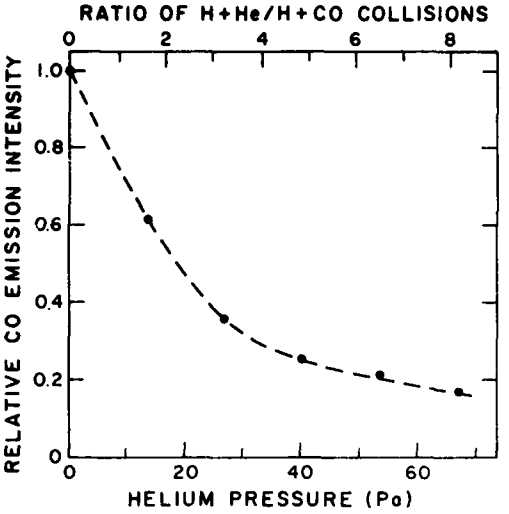

FIG. 7. Relative CO emission intensity following 193 nm photolysis of $H_2S/CO/He$ mixtures as a function of added helium pressure. The partial pressures of H_2S and CO in the photolysis cell are 0.33 and 6.34 Pa, respectively. The emission intensities are recorded with the InSb detector and a broadband infrared filter. The cold gas filter cell is evacuated.

recognized when interpreting the results. For example, because the response time of the infrared detector is slower than the initial collision rate, it is not possible to determine vibrational state distributions that are characteristic of a single collision of the H or D atoms with a CO target molecule. Secondary and tertiary collisions at successively lower translational energies undoubtedly contribute to the vibrational population distributions shown in Table III and Fig. 6. In addition, H atoms may suffer a velocity changing collision with an H_2S molecule before encountering a CO molecule. The latter effect is minimized by keeping the concentration of H_2S at or below 5%. None of the CO vibrational excitation may be attributed to T–V collisions of the HS photodissociation fragment, since, by conservation of energy and momentum, this particle has at most 0.07 eV translational energy, which is less than one quantum of CO vibration.

In order to gain a semiquantitative indication of the relative importance of secondary collisions in the experiment, helium buffer gas is added to the H_2S/CO mixture in the flow tube. Helium is an efficient moderator of the H atom translational energy through elastic momentum transferring collisions. The average fraction of the translational energy lost to the buffer gas in each hard-sphere collision is given by

$$\overline{\Delta E}/E = 2m_1 m_2/(m_1+m_2)^2 \ , \qquad (8)$$

which depends only on the masses of the two particles.[20] At this level of approximation, a hydrogen atom loses about 80% of its initial energy in only four collisions with helium atoms. As helium is added to the mixture in the flow tube, the CO emission intensity decreases (Fig. 7) because helium competes effectively with CO to slow the H atoms. At a buffer gas pressure sufficient to reduce the CO emission intensity by half, the CO pressure is only one third of the helium pressure. If we take van der Waals radii for He, CO,[21] and H[22] atoms as a measure of the relative molecular dimensions, this means that the hydrogen atoms suffer only two collisions with CO for every four collisions with helium atoms under these conditions. It is therefore reasonable to conclude that CO is even more efficient than He for removing translational energy from the fast hydrogen atoms.

For the T–V experiment, this result has the consequence that the observed vibrational distribution is predominantly due to the first one or two collisions of the H atom with CO molecules. Because the secondary collisions are at lower energies, the observed distributions are probably weighted toward lower v's (especially $v=1$) compared to the distribution expected for single collisions. The populations in higher vibrational levels must come almost exclusively from the first collision.

C. Translational energy dependence of T–V excitation

When other hydrogen atom precursors and photolysis laser wavelengths are used to vary the initial H atom energy, the resulting CO emission intensity is not sufficiently strong to permit the full deconvolution of the vibrational populations. However, the relative vibrational energy in the CO molecules may be compared for different H atom energies by measuring the total emission intensity with the InSb detector and a broadband infrared filter. To a very good approximation, the emission intensity associated with each vibrational level is proportional to its Einstein coefficient (Table II) which, in turn, is very nearly proportional to the vibrational energy of the emitting level. As a consequence the total emission intensity is proportional to the total vibrational energy of the CO molecules, regardless of the actual population distribution among the levels.

The observed intensities are corrected for the different photolysis cross sections of the H atom precursors at 193 or 248 nm. To obtain the relative fraction of H atom translational energy that is ultimately converted to CO vibrational energy, the corrected relative intensities are divided by the initial H atom energy. This quantity is plotted in Fig. 8 as a function of initial H atom energy and shows that the efficiency of T–V energy transfer increases by more than 300% over the range 1.0–3.2 eV. Two points are given in Fig. 8 for the HI precursor at 248 nm because a bimodal distribution of H atom energies is produced in that experiment (see Table I). It is not possible to distinguish how much of the observed emission is attributable to the H atoms at each of the two initial energies, so both points are plotted as a result of a single observable. Bimodal distributions also occur for HBr and HI photolysis at 193 nm but only a single point is presented for each of these experiments since the quantum yields for excited state halogen atoms are small (Table I).

D. Classical trajectory calculations

A set of classical trajectory calculations is computed so that qualitative features of the T–V experi-

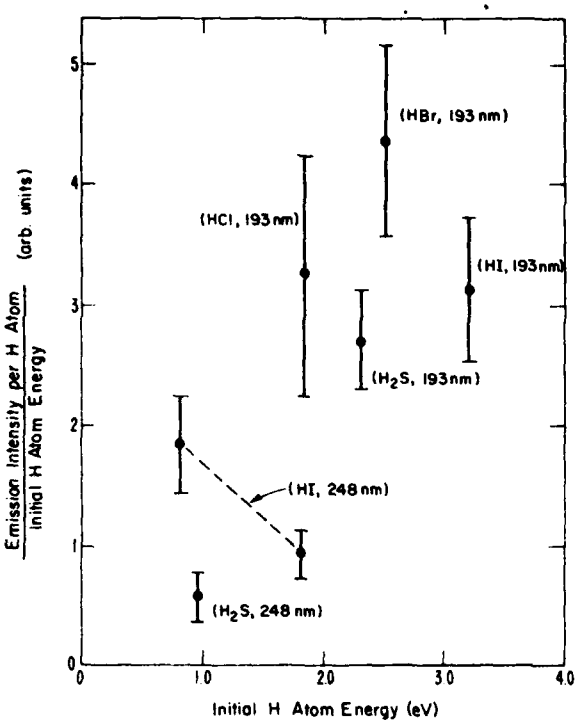

FIG. 8. Infrared emission intensity from CO following excitation by H atoms from photolysis of different precursors at 248 or 193 nm. The intensities are corrected for differences in photolysis cross sections of the precursors at the appropriate wavelengths and are then divided by the initial translational energy of the H atoms to show the energy dependence of T-V energy transfer efficiency. The intensity observed for photolysis of HI at 248 nm is represented by two points since a bimodal distribution of H atom energies is produced in that experiment (see the text).

ment can be correlated with theoretical predictions. The calculations are restricted to a collinear collision geometry and the CO molecule is treated as a classical harmonic oscillator that initially contains 1080 cm^{-1} of vibrational energy corresponding to the quantum mechanical zero point. The interaction potential energy function is assumed to be a simple repulsive exponential of the form

$$V(x) = A \exp(-x/L) \ , \tag{9}$$

where x is the distance between the H atom and the nearer atom of the CO molecule. For potential functions of this form, the dynamics of the calculation are independent of the value of A.[1] The characteristic length L is chosen to be 0.017 nm because in the energy range 0–3 eV, the potential closely resembles van der Waals potentials obtained from elastic scattering measurements of H atoms with CO at low energies.[22] Each trajectory is computed by numerically integrating the equation of motion of the three interacting particles until the H atom is far enough away from the CO oscillator that the collision can be considered "over." For each initial H atom energy, 31 trajectories are calculated for H + CO collisions corresponding to different initial phases of the oscillator. An additional 31 trajectories are computed for the opposite collision geometry (H + OC). The curves in Fig. 9 represent the average fraction of the H atom (or D atom) energy that is converted to classical CO vibration for all 62 trajectories.

Several interesting aspects of the calculations are *worth noting. At very low translational energies,* the classical oscillator gives up some energy to translation. This occurs to a greater extent for H + CO than for D + CO. Between 0.3 and 1.2 eV, the translation-to-vibration excitation with H atoms is more efficient than D atoms. At energies greater than 1.2 eV the fraction of translational energy that is converted to vibration approaches a constant value. Excitation by deuterium atoms is more efficient in this range because momentum coupling between the heavier D atom and diatomic oscillator is greater when the masses of the interacting particles are more nearly the same. At low energies, the greater efficiency of the H atoms for converting energy between translation and vibration may be ascribed to their higher velocity relative to D atoms at the same energy.

Semiclassical formulations of T–V energy transfer efficiency also make the same prediction of a decreasing velocity dependence with increasing translational energy.[1,2] The probability of exciting the $v = 0 \rightarrow 1$ transition *is proportional to the Fourier component of the time* varying interaction potential at the frequency of the diatomic oscillator. As the velocity of the particle increases, the collision becomes "sudden" with respect to the motion of the oscillator and the Fourier component at the oscillator frequency is proportional to the relative translational energy of the collision partners. Although semiclassical treatments such as Landau–Teller theory[23] have been quite successful for describing V–T relaxation at low collision energies, quantitative predictions are unreliable at energies greater than a few tenths of an electron volt due to terms which are neglected in the formulation of the theory.[2] It should

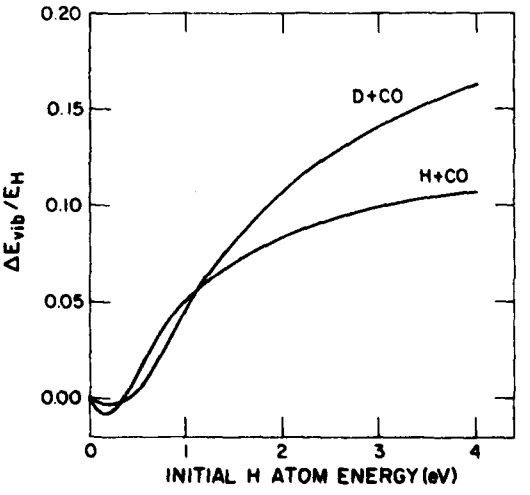

FIG. 9. Calculated T-V energy transfer for H + CO and D + CO collisions as a function of translational energy. For details of the classical trajectory calculations, see the text.

be noted that by restricting the calculations to collinear geometries, we have neglected possible effects of CO rotation in the T–V processes. Collision geometries which can lead to high rotational excitation (T–R) in the CO molecules are not considered. Keeping this in mind, we may qualitatively compare the results in Figs. 8 and 9 where the relative T–V efficiency is plotted as a function of initial H atom energy. It is gratifying to see that in both plots, the fraction of energy converted to CO vibration increases in the region 1–3 eV. A somewhat stronger energy dependence is observed in the experiments than is predicted by the calculations. It may be that the relative velocity dependence of T–V efficiency is underestimated in the calculations compared with the experiments because the collision geometry is restricted to be collinear. Alternatively, the collinear calculations may not correctly predict the energy at which the T–V efficiency levels off.

IV. DISCUSSION

Considering the total energy available in the collision between the fast H atom and the CO molecule, the vibrational energy observed in the target molecules is quite modest. For example, the 2.3 eV hydrogen atoms from 193 nm photolysis of H_2S could conceivably excite CO directly to the $v=9$ level. The experimental results, however, show that the excited level with the highest population is $v=1$. The populations of the higher vibrational states drop off rapidly with increasing quantum number and there appears to be no significant population above $v=5$ or $v=6$. Since the populations are derived from analysis of infrared emission intensities, there is no direct probe of the population remaining in the ground state. This trend of decreasing population with increasing quantum number is in agreement with other experimental and theoretical studies of T–V energy transfer.[6,11]

The vibrational population distributions resulting from H atom and D atom excitation at 2.3 and 2.2 eV, respectively, are the same within experimental uncertainty. Yet the absolute emission intensity, which is a more sensitive probe of the overall excitation efficiency, is 2.8 times greater using the lighter H atoms. This observation is in constrast to the results of the classical calculations, which predict that for collinear collision geometries, the heavier D atoms should be more efficient above 1.2 eV. Figure 8 shows that the fraction of energy converted from translation-to-vibration increases dramatically in the range 1–3.2 eV. The fact that this energy dependence is stronger than predicted by the classical calculations suggests that for most collision geometries, the coupling between the translation and vibration is still very sensitive to the relative velocity of the particles. This may explain, in part, the greater T–V efficiency of the H atoms.

A second consideration which may contribute to the greater overall efficiency of H atom excitation is the effects of multiple collisions. The helium buffer gas experiments show that CO is a more efficient moderator of the fast H atoms than He. At a buffer gas pressure sufficient to reduce the CO emission intensity to half its maximum value, the H atoms suffer twice as many collisions with He than with CO. Only a small fraction of the energy transfer may be attributed to momentum transferring (T–T) collisions because of the large difference between the masses of H and CO. The bulk of the transferred energy must be divided between vibrational (T–V) and rotational (T–R) excitation of the CO molecules. On the basis of the results in Fig. 7 and the calculated energy transfer to He in Eq. (8), more than 80% of the H atom energy appears to be transferred to CO in the first two collisions. The average internal energy of a CO molecule that has suffered one of these collisions would be in excess of 0.9 eV. This energy corresponds to 3.4 vibrational quanta. The observed population distributions place an upper limit of only 0.4 eV on the average vibrational energy in CO molecules that have undergone a collision with an H atom. This value assumes that the population in $v=0$ is zero; in fact the average vibrational energy is expected to be much less than this value. In any case it is apparent that a very large fraction of the H atom energy must be converted to rotational excitation of the CO molecules. High rotational excitation in H + CO collisions was recently reported by Wood, Flynn, and Weston.[24] Because the velocity of both H and D atoms is fast compared with rotational motion in the CO target molecules, the D atoms are expected to lose a greater fraction of their translational energy due to better momentum coupling. Thus the influence of multiple collisions on the overall excitation efficiency is probably more significant for H atom excitation because secondary and tertiary collisions occur at higher energies compared with D. This effect is further enhanced by the fact that as the H atoms lose energy, their relative T–V efficiency remains greater compared with D atoms, due to their greater velocity. For these reasons, the overall excitation efficiency is a much more sensitive indicator of the T–V probability than the vibrational distribution.

How well should classical models for collinear collisions predict the experimental observations? We might expect that the efficiency of T–V energy transfer scales roughly as the component of the H atom momentum along the CO internuclear axis.[25] Excitation to the higher vibrational levels probably comes primarily from "end on" collisions, whereas "broadside" geometries might lead to high rotational excitation and comparatively little vibrational energy transfer. Because the experiments quantify only the vibrational excitation, it is reasonable to expect that an experimental bias exists in favor of detecting collisions at small angles between the H atom velocity vector and the CO internuclear axis. Ideally, one would like to compare these results with three-dimensional quantum mechanical calculations describing the H + CO interaction. Although calculational methods to treat atom-diatomic[26] and atom-triatomic[27] systems have been developed, we are not aware of any results for H + CO or D + CO in the energy region 1–3.2 eV. Semiclassical models such as the Landau–Teller formalism have been developed using first-order perturbation theory, but these models are not valid at the high translational energies used in this study. For example, the probability of exciting

$v = 0 \rightarrow 1$ in a collinear H + CO collision at 2.3 eV is predicted by Landau–Teller theory to be greater than unity, a physically unrealistic result. Further, this theory predicts that the selection rule for T–V collisions is $\Delta v = +1$. Qualitatively, we can see that this prediction is fulfilled since most of the vibrationally excited molecules are in $v = 1$ (Fig. 6). There is, however, significant population in $v = 2, 3, 4$ and perhaps $v = 5$.

So far, we have not been able to address directly the question of how chemical forces influence the T–V process. The potential surface of the HCO radical has been the subject of several theoretical studies. The ground state of HCO has a bent configuration and the dissociation energy to H and CO is 17 kcal/mol.[28] Dissociation proceeds by means of an avoided electronic curve crossing to a repulsive $^2A'$ state which correlates with the ground states of the dissociation products. The activation energy for the reverse (association) reaction is believed to be about 2 kcal/mol as determined by the measurement of the gas phase termolecular recombination rate of H and CO.[29] The HOC radical surface is also believed to have a local minimum with a bent configuration, but this species is not stable with respect to dissociation.[30] These features of the potential surface are small in comparison with the initial H atom energies in these experiments. Also, attractive forces with chemical origins are generally highly directional, in contrast to repulsive forces which have less angular dependence. Few of the H + CO collisions can be expected to have a geometry such that the full attractive force of the C–H bond can be felt. Most theoretical studies of T–V interactions consider only the repulsive part of the potentials.

Secrest and Johnson have calculated exact quantum mechanical transition probabilities for collinear T–V interactions.[31] They find that "softening" the potentials by increasing L, the range parameter [Eq. (9)], leads to a decrease in the excitation probabilities. This observation is in general agreement with similar conclusions that may be drawn from the Landau–Teller[23] semiclassical formalism describing T–V interactions. According to the semiclassical theory, the $v = 0 \rightarrow 1$ transition probability is proportional to the square of the Fourier component of the time varying potential at the frequency of the molecular oscillator. Softening an exponential repulsion by increasing L shifts the Fourier transform spectrum of the collision to lower frequencies and simultaneously results in lower transition probability. The presence of deep potential wells in the surface, on the other hand, might increase the transition probabilities because the potential would be changing faster during the collision. Detailed examination of the effect of chemical attractive forces will depend both on refined theoretical characterization of T–V energy transfer and on experiments in which state selection and collision geometries are better defined. Some of the gross features of T–V energy transfer between H atoms and CO may be predicted using simple theoretical models and purely repulsive interaction potentials. Chemical forces may have subtle influences which are not obvious at the present level of the theory or experiment, but it appears that they may not play a significant role in dynamics of the T–V collisions in this case.

ACKNOWLEDGMENTS

The authors gratefully acknowledge the support of the U. S. Army Research Office and the National Science Foundation. They thank Frank Magnotta for his valuable preliminary experiments on this system.

[1]For a general discussion of vibrational relaxation, see J. T. Yardley, *Introduction to Molecular Energy Transfer* (Academic, New York, 1980).
[2]J. D. Lambert, *Vibrational and Rotational Relaxation in Gases* (Clarendon, Oxford, 1977).
[3]J. P. Toennies, Annu. Rev. Phys. Chem. 27, 225 (1976).
[4]G. Flynn and E. Weitz, Annu. Rev. Phys. Chem. 25, 275 (1974).
[5]F. Linder, in *Electronic and Atomic Collisions*, edited by N. Oda and K. Takayanagi (North–Holland, Amsterdam, 1980), p. 535.
[6]M. Faubel and J. P. Toennies, Advan. At. Mol. Phys. 13, 229 (1977).
[7]F. Magnotta, D. J. Nesbitt, and S. R. Leone, Chem. Phys. Lett. 83, 21 (1981).
[8]C. R. Quick, Jr., R. E. Weston, Jr., and G. W. Flynn, Chem. Phys. Lett. 83, 15 (1981).
[9]S. R. Leone, Acc. Chem. Res. (in press).
[10]G. P. Glass and S. Kironde, J. Phys. Chem. 86, 908 (1982).
[11]J. Krutein and F. Linder, J. Chem. Phys. 71, 599 (1979).
[12]G. Drolshagen, F. A. Gianturco, and J. P. Toennies, J. Chem. Phys. 73, 5013 (1980).
[13]H. Okabe, *Photochemistry of Small Molecules* (Wiley-Interscience, New York, 1978); P. Cadman and J. C. Polanyi, J. Phys. Chem. 72, 3715 (1968).
[14]W. G. Hawkins and P. L. Houston, J. Chem. Phys. 73, 297 (1980). Recent work by A. E. deVries *et al.*, Chem. Phys. (to be published) finds 10.5% vibrational excitation of SH at 193 nm.
[15]K. P. Huber and G. Herzberg, *Molecular Spectra and Molecular Structure IV. Constants of Diatomic Molecules* (Van Nostrand Reinhold, New York, 1979).
[16]L. A. Young and W. J. Eachus, J. Chem. Phys. 44, 4195 (1966).
[17]M. F. Weisbach and C. Chackerian, Jr., J. Chem. Phys. 59, 4272 (1973).
[18]K. Watanabe and A. S. Jursa, J. Chem. Phys. 41, 1650 (1964).
[19]Y. S. Liu, R. A. McFarlane, and G. J. Wolga, J. Chem. Phys. 63, 228 (1975).
[20]R. N. Porter, J. Chem. Phys. 45, 2284 (1966).
[21]J. O. Hirschfelder, C. F. Curtiss, and R. B. Bird, *Molecular Theory of Gases and Liquids* (Wiley, New York, 1964).
[22]W. Bauer, R. W. Bickes, Jr., B. Lantzsch, J. P. Toennies, and K. Walaschewski, Chem. Phys. Lett. 31, 12 (1976); G. Caracciola, T. H. Ellis, G. O. Este, A. Ruffalo, G. Scoles, and U. Valbussa, Astrophys. J. 229, 451 (1979).
[23]L. Landau and E. Teller, Phys. Z. Sowjetunion. 10, 34 (1936); K. F. Herzfeld and T. A. Litovitz, *Absorption and Dispersion of Ultrasonic Waves* (Academic, New York, 1959).
[24]C. F. Wood, G. W. Flynn, and R. E. Weston, Jr., J. Chem. Phys. 77, 4776 (1982).
[25]J. A. Serri, R. M. Bilotta, and D. E. Pritchard, J. Chem. Phys. 77, 2940 (1982).
[26]R. Schinke and P. McGuire, Chem. Phys. 31, 391 (1978); R. Schinke, M. Dupuis, and W. A. Lester, Jr., J. Chem. Phys. 72, 3909 (1980); F. A. Gianturco, U. T. Lamanna, and M. Attimonelli, Chem. Phys. 48, 399 (1980).
[27]D. C. Clary, J. Chem. Phys. 75, 209 (1981); D. C. Clary,

Chem. Phys. Lett. 74, 454 (1980); D. C. Clary, J. Chem. Phys. 75, 3899 (1981); N. Mullaney Harvey, Chem. Phys. Lett. 88, 553 (1982); R. T. Skodje, W. R. Gentry, and C. F. Giese, J. Chem. Phys. 66, 160 (1977), and references therein.
[28]P. Warneck, Z. Naturforsch. A 29, 350 (1974).
[29]H. Y. Wang, J. A. Eyre, and L. M. Dorfman, J. Chem. Phys. 59, 5199 (1973).
[30]S. Carter, I. M. Mills, and J. N. Murrell, J. Chem. Soc. Faraday Trans. 2 75, 148 (1979); P. J. Bruna, R. J. Buenker, and S. D. Peyerimhoff, J. Mol. Struct. 32, 217 (1976).
[31]D. Secrest and B. R. Johnson, J. Chem. Phys. 45, 4556 (1966).